

Charge-Carrier Density Independent Mobility in Amorphous Fluorene-Triarylamine Copolymers

Alasdair J. Campbell,* Ruth Rawcliffe, Alexander Guite, Jorge Costa Dantas Faria, Abhimanyu Mukherjee, Martyn A. McLachlan, Maxim Shkunov, and Donal D. C. Bradley

A charge-carrier density dependent mobility has been predicted for amorphous, glassy energetically disordered semiconducting polymers, which would have considerable impact on their performance in devices. However, previous observations of a density dependent mobility are complicated by the polycrystalline materials studied. Here charge transport in field-effect transistors and diodes of two amorphous, glassy fluorene-triarylamine copolymers is investigated, and the results explored in terms of a charge-carrier density dependent mobility model. The nondispersive nature of the time-of-flight (TOF) transients and analysis of dark injection transient results and transistor transfer characteristics indicate a charge-carrier density independent mobility in both the low-density diode and the high-density transistor regimes. The mobility values for optimized transistors are in good agreement with the TOF values at the same field, and both have the same temperature dependency. The measured transistor mobility falls two to three orders of magnitude below that predicted from the charge-carrier density dependent model, and does not follow the expected power-law relationship. The experimental results for these two amorphous polymers are therefore consistent with a charge-carrier density independent mobility, and this is discussed in terms of polaron-dominated hopping and interchain correlated disorder.

1. Introduction

Organic semiconductors (OSCs) such as conjugated polymers can be used in a range of different optoelectronic devices, including organic light emitting diodes (OLEDs), organic photovoltaics

(OPVs), and organic field-effect transistors (OFETs). A crucial parameter in the development of these technologies is the OSC charge-carrier mobility, and how it is related to the different OSC materials, processing, device architectures, and device operating conditions. Many semiconducting polymers and small molecules are amorphous, and such disorder in the physical morphology is expected to reflect itself in disorder of the energy levels of the hole and electron transport states (Figure 1a). Such energetic disorder will directly impact charge transport and mobility.^[1–12]

For such energetically disordered OSCs, one feature predicted by many charge transport models is a charge-carrier density dependent mobility. The original Gaussian disorder model (GDM) developed by Bässler for hopping transport in a Gaussian density of states (DOS) distribution was a single carrier approach,^[1] as were the models based on it which considered both correlated energetic disorder,^[2] with a smoothly varying energy landscape (see Figure 1a), and the effect of polaronic relaxation.^[3] The percolation model developed by Vissenberg and Matters for transport involving an exponential DOS instead considered multiple carriers,^[4] and this predicted a mobility which has a power-law dependency on the charge-carrier density.^[5]

Dr. A. J. Campbell, Dr. R. Rawcliffe, Dr. A. Guite,
J. Costa Dantas Faria, A. Mukherjee,
Prof. D. D. C. Bradley,^[†]
Department of Physics and the
Centre for Plastic Electronics
Imperial College London
Blackett Laboratory
South Kensington Campus
London SW7 2AZ, UK
E-mail: alasdair.campbell@imperial.ac.uk

Dr. M. A. McLachlan
Department of Material Science and the Centre for Plastic Electronics
Imperial College London
South Kensington Campus
London SW7 2AZ, UK

Dr. M. Shkunov
Advanced Technology Institute
Electronic and Electrical Engineering
University of Surrey
Guildford, Surrey GU2 7HX, UK

^[†]Present address: Departments of Engineering Science and Physics, Division of Mathematical, Physical and Life Sciences, University of Oxford, 9 Parks Road, Oxford OX1 3PD, UK

This is an open access article under the terms of the Creative Commons Attribution License, which permits use, distribution and reproduction in any medium, provided the original work is properly cited.



DOI: 10.1002/adfm.201504722

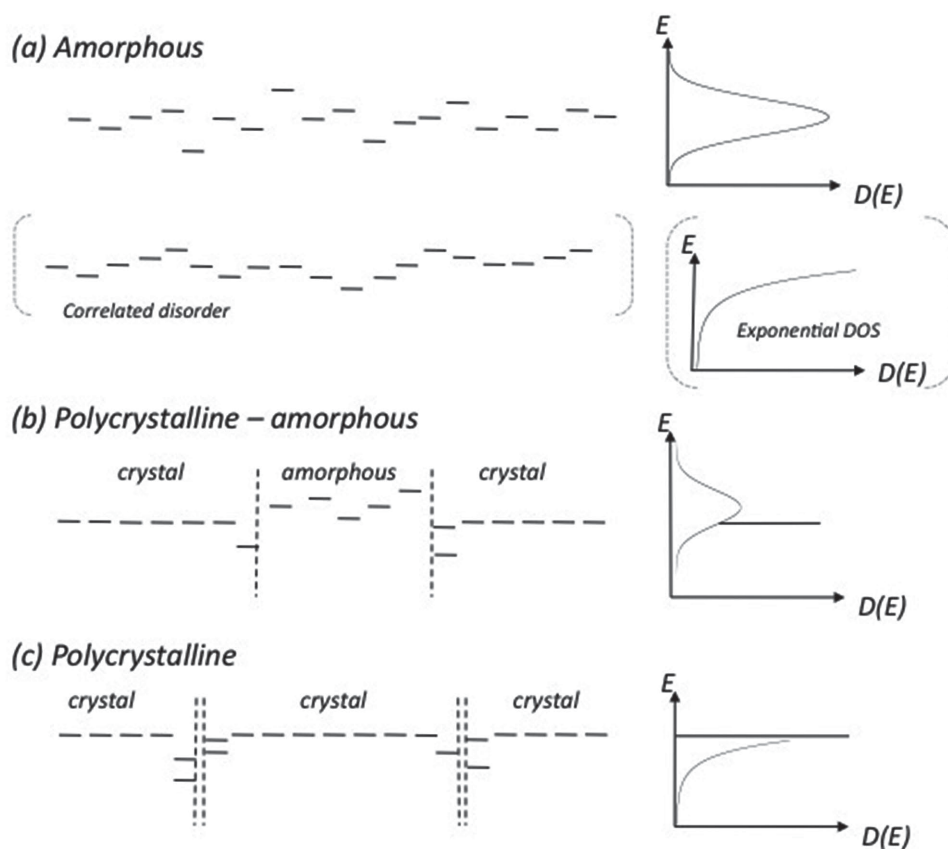


Figure 1. Representations of the transport state energy landscape and density of states (DOS) distribution $D(E)$ for different disordered organic semiconductors. a) A pure amorphous, glassy material with uncorrelated disorder and a Gaussian DOS. Also shown is the correlated disorder variant, where the energy of nearest-neighbor states forming a Gaussian DOS are not random (uncorrelated) but correlated. An exponential DOS is also sometimes used as an approximation to a Gaussian DOS. b) A mixed polycrystalline-amorphous system consisting of small crystallites or aggregates embedded in a varying fraction of amorphous material. c) A polycrystalline material consisting of only small crystallites.

Multiple carriers have additionally been included for various models involving a Gaussian DOS, such as the effective-median approximation theory,^[6] the extended GDM (EGDM),^[7] and a recent scaling theory percolation model.^[8] These again predict a mobility which increases with increasing charge-carrier density, additionally showing that the temperature dependency of charge transport should simultaneously decrease,^[9] and that correlated energetic disorder and polaronic effects will vary the behavior.^[6,8,10–12]

Experimentally, OFETs probe the high charge-carrier density regime between about 10^{17} and 10^{20} cm^{-3} , while diodes (OPVs and OLEDs) probe the low charge-carrier density between about 10^{15} and 10^{17} cm^{-3} . The total number of transport states (based on the molecular or conjugation length density) is about 5×10^{20} cm^{-3} , so in OFETs there is about 1 carrier per 10–100 sites, while in diodes there is about 1 carrier per 10 000–100 000 sites. Tanase et al. have investigated the charge-carrier density dependence of the mobility in poly(3-hexylthiophene) (P3HT) and different soluble poly(phenylene-vinylene) (PPV) copolymers in both OFETs and in diodes, the latter using steady-state space charge limited current (SCLC) measurements.^[5,13] The OFET results in the high-density regime could be fitted to the power-law dependency of mobility with carrier density predicted

by Vissenberg and Matters, and successfully linked to both the magnitude and Gaussian DOS width of the SCLC diode mobility in the low-density regime. Results for poly(2-methoxy-5-(2'-ethylhexyloxy)-1,4-phenylenevinylene) (MEH-PPV) OFETs and diodes indicate a power-law dependency extended across both regimes from 10^{15} to 10^{20} cm^{-3} .^[14] OFET measurements for pentacene and C60 in the high-density regime also indicate a mobility whose magnitude and temperature dependence vary with charge-carrier density.^[9] Transient mobility measurements of P3HT and poly(2,1,3-benzothiadiazole-4,7-diyl[4,4-bis(2-ethylhexyl)-4H-cyclopenta[2,1-b:3,4-b']dithiophene-2,6,diyl]) (PCPDTBT) in solar cells also indicate a charge-carrier density dependent mobility in the low-density regime from 2×10^{16} to 3×10^{17} cm^{-3} .^[15]

However, there is an intriguing discontinuity between the material systems envisaged by the models, and some of the above material systems used to test them.

The models have been developed for amorphous, glassy materials in which the energy landscape is either uncorrelated or correlated and forms a Gaussian or exponential DOS (see Figure 1a). In contrast, P3HT is polycrystalline, consisting of small crystals (aggregates) embedded in an amorphous fraction,^[16–18] and the diode mobility varies with film thickness as

the morphology changes.^[19] MEH-PPV films consist of ordered nanoscale domains (aggregates) embedded in amorphous material, diode mobility varying with film morphology.^[20–23] PCPDTBT films again consist of polycrystalline domains embedded in amorphous material.^[24] Pentacene and C60 form pure polycrystalline thin films.^[25,26] The energy landscape and DOS for such polycrystalline-amorphous blend systems and polycrystalline systems would be expected to differ considerably from that of a pure amorphous glass (see Figure 1b,c). Even at low crystalline fractions, charge transport is expected to deviate from that in a pure amorphous system, the crystals or aggregates acting as deep charge traps. At high crystalline fractions, transport will tend toward the pure polycrystalline materials, where tunneling between crystals and grain boundary charge trapping dominates. In such materials, one is entering a regime where mobility-edge models become much more physically reasonable.^[27–30]

To really test transport models based on amorphous materials therefore requires the use of amorphous, glassy organic semiconductors. Fluorene-triarylamine copolymers are specifically designed to be amorphous, with high glass transition temperatures, for use as interlayer and hole transport layer materials in polymer light emitting diodes.^[31–37] They have also been used, along with the homopolymer poly(triarylamine), as p-type semiconductors in OFETs, allowing highly uniform charge transport over large-area substrates, an important requirement for applications such as display backplanes.^[38] Their charge transport has been extensively studied in bulk diodes using the time-of-flight (TOF) and transient SCLC dark injection (DI) techniques,^[39–42] and modeled in the low charge-carrier density regime using the GDM, correlated GDM, and polaronic correlated GDM.^[43] More recently they have also been used to test the correlated and uncorrelated EGDM in the low charge-carrier density regime using steady-state SCLC diode measurements.^[44]

Here we investigate the charge-density dependence of the hole mobility across both the low and high charge-carrier density regimes in two fluorene-triarylamine copolymers, poly(9,9-dioctylfluorene-co-bis-*N,N'*-(4-butylphenyl)-bis-*N,N'*-phenyl-1,4-phenylenediamine) (PFB) and poly(9,9-dioctylfluorene-co-bis-*N,N'*-(4-methoxyphenyl)-bis-*N,N'*-phenyl-1,4-phenylenediamine) (PFMO). These have been chosen due to their low ionization potentials to minimize the impact of any charge injection effects on the measured mobility values. TOF measurements and analysis of literature transient SCLC dark injection results are used to investigate hole transport in the low-density diode regime, while OFET measurements are used to investigate the high-density transistor regime. The power-law dependency of the transistor mobility is calculated for the Vissenberg and Matters model from the TOF Gaussian DOS width, and compared to the measured OFET values. The temperature variation of the mobility from TOF and OFETs were additionally compared. Fascinatingly, the results indicate that hole transport in PFB and PFMO is charge-carrier density independent, the best performing transistors having mobility values equal to the diodes at the same field value despite the large differences in carrier density. We discuss the implications of these results in terms of charge transport in amorphous and polycrystalline organic semiconducting materials.

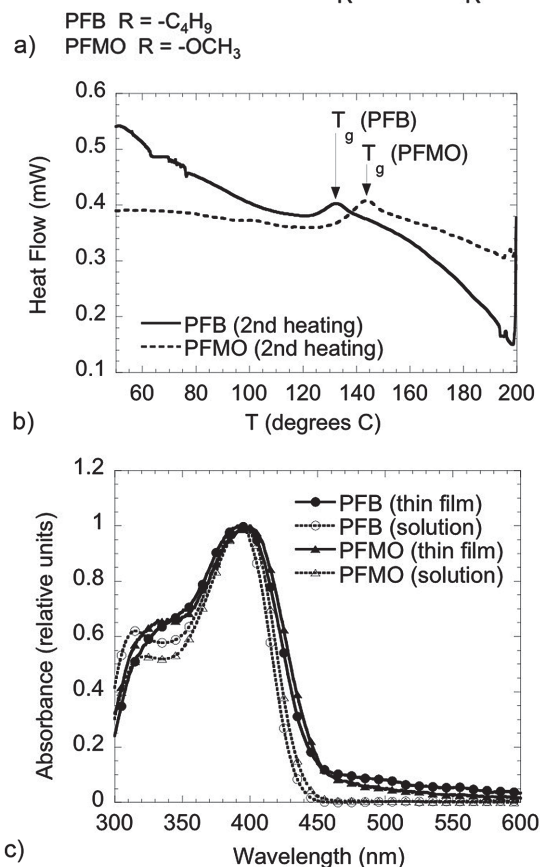
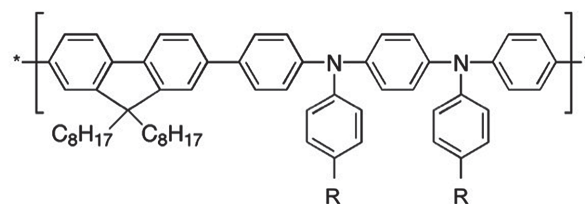


Figure 2. a) Chemical structure of PFB and PFMO. b) Differential scanning calorimetry (DSC) spectra of PFB and PFMO. This is for the 2nd heating run. c) Optical absorption spectra of PFB and PFMO solutions in toluene and thin-films.

2. Results and Discussion

We first explored the physical morphology of thin films of PFB and PFMO (chemical structure, **Figure 2a**). Differential scanning calorimetry (DSC) spectra (**Figure 2b**) are relatively featureless, showing a single broad, weak peak upon heating and cooling, which can be associated with the second-order glass transition temperature. These are very similar to that for TFB,^[36] and other fluorene-triarylamine copolymers are also found to only exhibit this second-order glass transition.^[38,45] This is very different from that of polycrystalline polymers such as P3HT, poly(9,9-dioctylfluorene) (PFO), poly(9,9-dioctylfluorene-*alt*-benzothiadiazole) (F8BT), and poly(9,9-dioctylfluorene-*alt*-bithiophene), which can have rich and complex DSC spectra showing multiple peaks from glass, crystallization, and melting transitions.^[36,46–51] The thin film optical absorption spectra of PFB and PFMO (**Figure 2c**) are broad and featureless, and strongly

resemble the solution spectra using a good solvent in which the chains are in the random-coil conformation. This is exactly as for TFB, being an expected characteristic of an amorphous semiconducting polymer.^[36] Polycrystalline polymers such as P3HT, F8BT, and PFO instead typically show a red shift of the absorption edge and/or more structure with vibrational sideband detail in their thin film spectra compared to the good-solvent solution spectra.^[17,36,47,48,52–54] We additionally recorded the X-ray diffraction (XRD) data (Figure S1, Supporting Information) of a 330 nm thick film of PFB annealed for 1 h at 150 °C just above the glass transition temperature to encourage any potential crystallite formation (PFMO was not investigated due to limited material availability). Despite a relatively long scan time, the diffractogram showed no diffraction peaks, the spectrum being dominated by the background due to the glass substrate (we note that F8BT films show clear diffraction peaks under the same experimental conditions with the same apparatus (see the Supporting Information of ref.^[33])). This is consistent with XRD results for TFB and other fluorene-triarylamine copolymers, which show no evidence of any crystalline phase.^[38,55] The DSC, optical absorption, and XRD results are therefore consistent with PFB and PFMO being amorphous, glassy polymers.

To investigate hole transport in PFB and PFMO in the low-carrier density diode regime, we use the TOF technique to measure the nature of transport and its field dependence, and analyze transient SCLC dark injection and TOF results to find the charge-carrier density dependence over the same field range. To investigate hole transport in the high-carrier density diode regime, we use bottom-gate bottom-contact OFETs in both conventional linear and saturation regimes and the low field linear regime, the latter to generate a highly uniform charge-carrier density across the length of the channel.^[5] To replicate the original studies by Tanase et al. on P3HT and PPV copolymers,^[5,13] OFET samples consisted of standard Si (n^+ doped)/SiO₂ wafer substrates with Au source and drain contacts, with and without contact and channel self-assembled monolayers (SAMs).

One important factor in these types of measurements is to eliminate as far as possible the impact of injection on the measured mobility values. Steady-state SCLC measurements can potentially underestimate the bulk mobility by up to an order of magnitude due to interfacial traps at the polymer/electrode interface.^[32] The TOF technique does not involve injection, so avoids this issue. The transient SCLC dark injection technique is based on a transit time like the TOF technique; it is

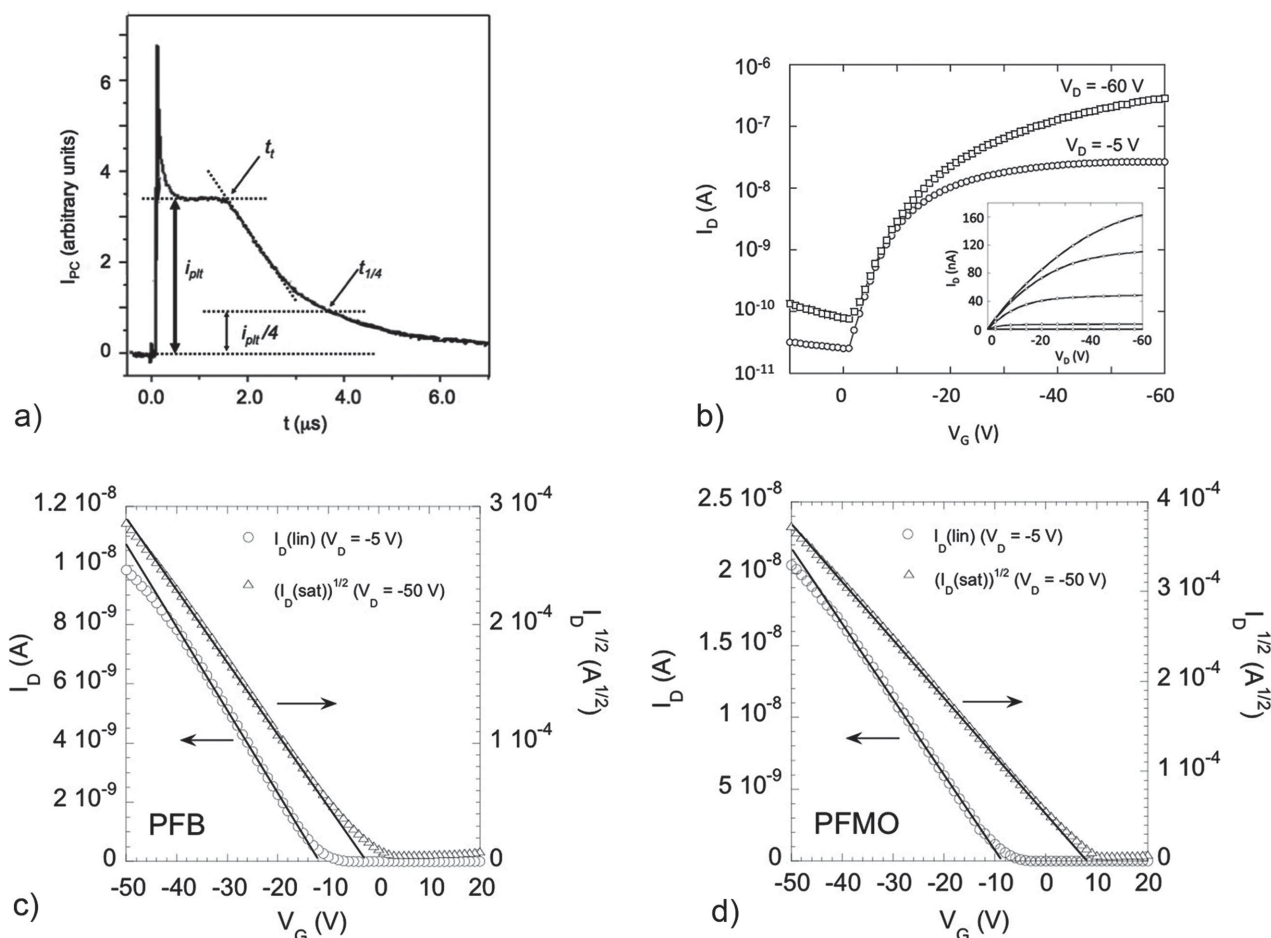


Figure 3. a) Representative time-of-flight (TOF) transient for hole transport in PFB. b) Representative transfer characteristics for a PFB field-effect transistor. Inset shows output characteristics (between $V_G = 0$ and -60 V at -15 V intervals). c,d) Variation of the linear regime drain current $I_D(\text{lin})$ and the square-root of the saturation regime drain current $(I_D(\text{sat}))^{1/2}$ with gate voltage V_G for c) PFB and d) PFMO. Lines are fits to Equations (2a) and (3b).

independent of the magnitude of the current signal, which could potentially be reduced by injection efficiency effects.^[32] However, we use the SCLC equation to calculate the charge-carrier density for the dark injection measurements, and contact resistance effects can also lower the transistor mobility. To avoid this, PFB and PFMO have been selected amongst the fluorene-triarylamine copolymers as they have low ionization potentials of 5.09 and 4.98 eV, respectively, minimizing the injection barrier with the diode and transistor contacts used in this work.^[31] The relatively low mobility of both materials ($\leq 10^{-3} \text{ cm}^2 \text{ V}^{-1} \text{ s}^{-1}$) also indicates that for the OFETs, the channel resistance should dominate over any contact effects. To check any possible injection effects, we also investigated devices with and without an injection barrier lowering thiol SAM attached to the Au source and drain contacts.

We also wish to compare the low and high carrier density regimes in diodes (transport vertically through the thin films) and OFETs (transport horizontally at the interface of the thin films). In polycrystalline materials, there is no guarantee that the amount of crystallinity, or the crystal size and orientation, will be the same in the bulk film as it is at the interface with a dielectric. Any difference could make charge transport anisotropic, making it difficult to compare results in diodes and OFETs. We note that the amorphous nature of PFB and PFMO avoids this problem, any differences in bulk or interfacial morphology being minimized.

Figure 3a shows typical room temperature hole TOF transients for PFB. Similar results were obtained for PFMO. The TOF transients are nondispersive and show a clear transit time, in good agreement with previous measurements.^[31,39,41] Nondispersive transport indicates that the sheet of photogenerated carriers has reached equilibrium within the transport site DOS distribution as it transits the film.^[1] All of the carriers have therefore sampled the deep sites within the DOS. This is in contrast to charge-density dependent transport, in which deep site filling results in many carriers not entering these sites and therefore moving faster. This would also make transport dispersive as the deep sites slowly empty. The shape of the PFB and PFMO TOF transients therefore indicates that the transport in the low-density diode regime is not charge-carrier density dependent.

We note that this is supported by transient SCLC dark injection measurements of PFB in the literature. In SCLC measurements, the average charge-carrier density in the diode is inversely proportional to the device thickness, and this can be used to test carrier density dependent mobility models.^[56] Results for PFB have measured the transient SCLC dark injection mobility over a range of thicknesses from 200 to 1100 nm.^[39,40] Across a wide range of field values, the dark injection mobility for PFB does not change with device thickness. Hence, the mobility in these diodes must be independent of carrier density.

Figure 3b shows typical room temperature OFET transfer and output characteristics for PFB (for PFMO, see Figure S2, Supporting Information). The transistors show well-behaved characteristics, with clear linear and saturation regimes.

The TOF mobility was calculated from $\mu_{\text{TOF}} = d/(t_{\text{trans}}F)$ where t_{trans} is the charge-carrier transit time and $F = V/d$ where V is the applied bias and d is the device thickness. The transit time can be taken as the inflexion point time t_i (where the photocurrent starts

to decrease from the constant current plateau) (see Figure 3a). However, in previous measurements of PFB, the transit time taken as the quarter-height time $t_{1/4}$ (when the current reaches quarter the plateau value) (see Figure 3a) gave the best agreement with the mobility calculated from transient dark injection measurements for all diode thicknesses between 220 and 1100 nm.^[39] To cover all possibilities, we have calculated the TOF mobility from both t_i and $t_{1/4}$ (the half-height transit time $t_{1/2}$, when the current reaches half the plateau value, will lie between these values). According to the GDM and the correlated GDM, the TOF mobility should be field dependent with the form

$$\mu(F) = \mu_0 \exp A\sqrt{F} \quad (1)$$

where μ_0 is the zero-field mobility, F is the field, and A is a constant.^[1,2] The $\mu_{\text{TOF}}(t_0)$ and $\mu_{\text{TOF}}(t_{1/4})$ results are shown in Figure 4a and fitted to Equation (1).

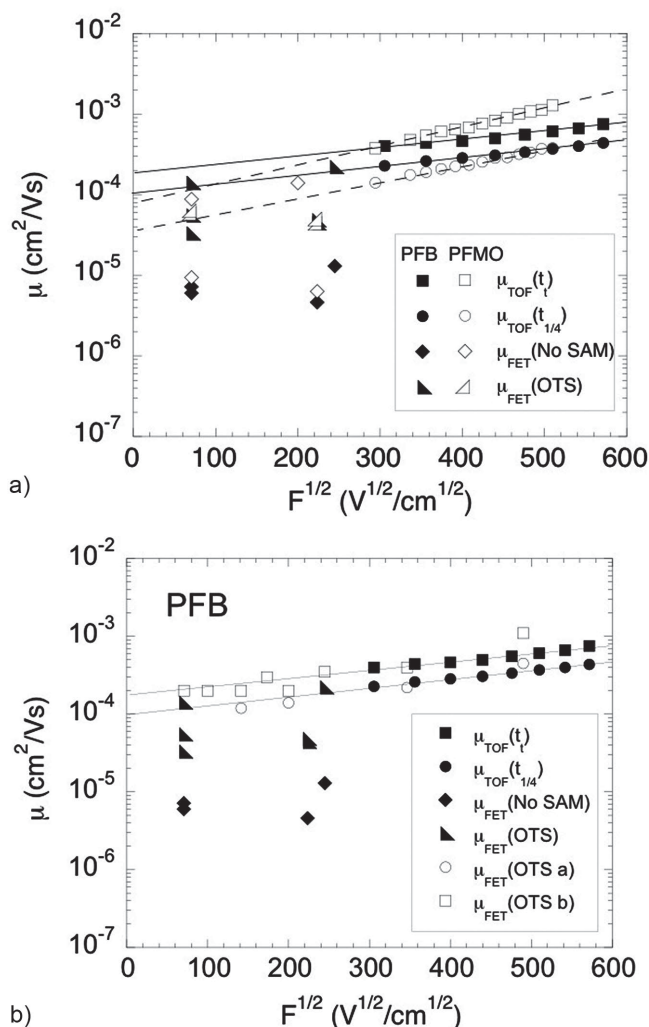


Figure 4. a) Variation of PFB and PFMO TOF and linear and saturation field-effect transistor (FET) mobility μ with the square-root of the applied field F . Solid and dashed lines are fits of Equation (1) to the TOF results. b) As 4a) for PFB but including additional data for transistors with a range of different channel lengths ($L = 2.5, 5, 10, \text{ and } 20 \mu\text{m}$). OTS a and OTS b are from two different device fabrication runs.

To extract the standard values for the field-effect transistor (FET) mobility μ_{FET} , the linear and saturation transfer characteristics were fitted to the standard transistor equations

$$I_D(\text{lin}) = \frac{W\mu_{\text{FET}}C_i}{L}(V_G - V_T)V_D \quad (2a)$$

$$I_D(\text{sat}) = \frac{W\mu_{\text{FET}}C_i}{2L}(V_G - V_T)^2 \quad (2b)$$

on a $I_D(\text{lin})$ versus V_G and $(I_D(\text{sat}))^{1/2}$ versus V_G plot (Figure 3c,d), where $I_D(\text{lin})$ and $I_D(\text{sat})$ are the linear and saturation drain currents, respectively, V_G is the gate bias, V_T the turn-on voltage, V_D the drain bias, W the channel width, L the channel length, and C_i is the insulator capacitance per unit area. Values are plotted in Figure 4a for field values of $F = V_D/L$, where L is the channel length. Values for octyltrichlorosilane (OTS) treated devices $\mu_{\text{FET}}(\text{OTS})$ tend to be higher than those for devices with no channel SAM $\mu_{\text{FET}}(\text{No SAM})$, although there are exceptions. This is consistent with OTS providing a more controllable dielectric surface with better wetting properties than bare SiO_2 .^[57] The variation of $\mu_{\text{FET}}(\text{OTS})$ with F for PFB over a range of fields is shown in Figure 4b. The transistor mobility appears to follow Equation (1) and is in good agreement with the variation found for the TOF results. Devices with the contact thiol SAM 4-fluorothiophenol (FTP) for PFB and PFMO had mobility values similar to devices with only the bare contacts $\mu_{\text{FET}}(\text{No SAM})$ (see Figure S3, Supporting Information). The linear mobility for PFB was also found to remain constant as L was varied from 2.5 to 20 μm , and transmission line method analysis to calculate the linear mobility in the absence of contact resistance gave the same value (Section S4 and Figure S4a,c, Supporting Information). This indicates that if any contact resistance effects are present they are having minimal impact on the extracted mobility for these two low ionization potential polymers at the V_D values used in Figure 4a,b.

The results in Figure 4a,b show two important features. First, for all devices measured, μ_{FET} is approximately equal to or greater than μ_{TOF} at the same field. This is inconsistent with all the charge-carrier density dependent models, which predict that $\mu_{\text{FET}} \gg \mu_{\text{TOF}}$ (the charge-carrier density in transistors should be orders of magnitude above that in diodes). Second, for the best performing transistors, $\mu_{\text{FET}}(F) \approx \mu_{\text{TOF}}(F)$. This suggests that in optimised transistors, charge transport at the interface is identical to that in the bulk. This is a characteristic of a charge-carrier density independent mobility.

We then measured the variation of μ with charge-carrier density p in both diodes and transistors, and explored these results within the Vissenberg and Matters framework using the model developed by Tanase et al.^[5]

For the diodes, transient dark injection SCLC and TOF mobility values μ_{DI} and μ_{TOF} for device thicknesses between 200 and 1750 nm and three different field values (100, 200, and 300 kV cm^{-1}) were taken from previous literature measurements.^[39–41] The average dark injection hole density p_{DI} was calculated according to SCLC theory using the equation

$$p_{\text{DI}} = \frac{3 \epsilon_r \epsilon_0 F}{2 e d} \quad (3)$$

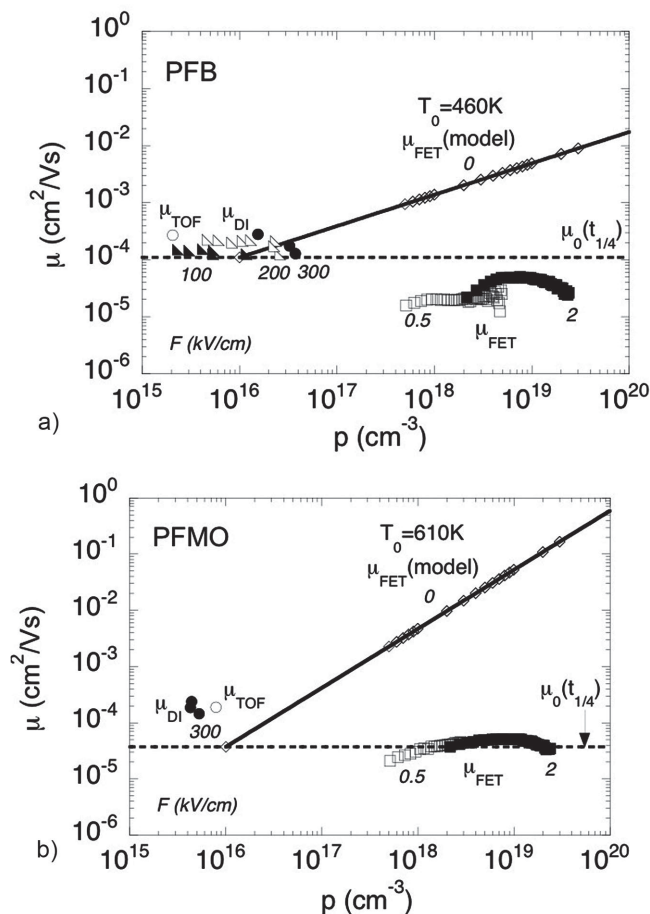


Figure 5. Variation of the dark injection (DI), TOF, and FET hole mobility μ with charge-carrier density p for a) PFB and b) PFMO. Numerical values in italics indicate the applied field F in kV cm^{-1} . Horizontal dashed lines, equal to the zero-field TOF mobility $\mu_0(t_{1/4})$, are for a p -independent FET mobility. Solid lines and $\mu_{\text{FET}}(\text{model})$ are for the p -dependent FET mobility model (at zero-field) in ref.^[5]. DI and TOF hole mobility values are taken from refs.^[39–41].

where ϵ_r and ϵ_0 are the relative dielectric and vacuum permittivity, respectively, and e is the charge on the electron (we take $\epsilon_r = 3.5$). The TOF carrier density was calculated from the total charge in the measured transient and assuming a photogenerated charge sheet thickness equal to the absorption depth (≈ 100 nm). (The results of this analysis for PFB at three different field values are shown in Figure S5 in the Supporting Information. As discussed above, these clearly indicate a charge-carrier density independent mobility in the low carrier density diode regime.)

For the transistors, it is important to measure the mobility in the low drain bias regime to achieve a uniform charge density along the length of the channel. The linear-regime transfer characteristics for PFB and PFMO transistors were measured at drain bias V_D values of -0.5 and -2 V. The linear-regime FET mobility was calculated as previously described.^[5] The FET charge-carrier density per unit volume was calculated from

$$p_{\text{FET}} = \frac{-C_i(V_G - V_0 - V_D / 2)}{e\Delta x} \quad (4)$$

where V_0 is the gate voltage where the device turns on (i.e., the drain current exceeds the off current), and Δx is the channel depth (which we take as 2 nm from work by the authors of the approach^[5,13]). Data are only plotted for $V_G - V_0 \geq 2V_D$ to maintain a uniform charge density in the channel. p_{FET} values varied from 5×10^{17} to $3 \times 10^{19} \text{ cm}^{-3}$, covering the range previously studied.^[5,13] Note that for $V_D = -0.5 \text{ V}$, data could only be recorded for the higher mobility transistors. It also became very noisy above p_{FET} values of $3 \times 10^{18} \text{ cm}^{-3}$, so has not been plotted above this point. Additionally, the lower limit of $5 \times 10^{17} \text{ cm}^{-3}$ is set by the inaccuracy in estimating V_0 of about $\pm 0.5 \text{ V}$. In PFB, $V_D = -0.5 \text{ V}$ also gave a slightly lower mobility value than $V_D = -2 \text{ V}$, most likely due to injection effects at the low field. This was not an issue for PFMO, which has a smaller ionization potential than PFB.

Dark injection, TOF, and representative transistor mobility results are plotted against charge density in Figure 5a,b for PFB and PFMO, respectively. The horizontal dashed line is the zero-field mobility $\mu_0(t_{1/4})$.

To fit our results to the model of Tanase et al., we require the Gaussian transport DOS width σ_{DOS} for PFB and PFMO. This has been measured within our group using the variation of the TOF mobility with field and temperature.^[39,58] Analysis using the Bässler GDM gives values for the PFB and PFMO DOS width of 0.085 and 0.11 eV, respectively.^[1,39,58] Converting to the correlated GDM (a factor of 10/9) gives values of σ_{DOS} of 0.094 and 0.12 eV, respectively.^[1,2] To find the Vissenberg and Matters exponential DOS distribution characteristic temperature T_0 , we use the comparative method used by Tanase et al. We take a Gaussian DOS distribution with a total integrated site density of $N = 3 \times 10^{20} \text{ cm}^{-3}$ and width σ_{DOS} from the correlated GDM.^[5] We integrate across the distribution and the Fermi–Dirac function at room temperature to find the position of the Fermi level at the minimum and maximum values of p_{FET} . We then fit the Gaussian DOS between these two values to an exponential DOS of form $N_{\text{exp}} \exp(-E/k_B T_0)$ where E is energy, N_{exp} density, and k_B is Boltzmann's constant. This results in values of T_0 of 460 and 610 K for PFB and PFMO, respectively. $\mu_{\text{TOF}}(t_{1/4})$ gives the best agreement with the bulk SCLC dark injection mobility.^[39] Therefore, by extrapolation from $\mu_0(t_{1/4})$ at 10^{16} cm^{-3} , we use these values of T_0 to calculate the values of the FET mobility $\mu_{\text{FET}}(\text{model})$ predicted by the model using

$$\mu_{\text{FET}}(\text{model}) = \mu_0 \left(\frac{p_{\text{FET}}}{p_0} \right)^m \quad (5)$$

$$m = \frac{T_0}{T} - 1$$

where μ_0 and p_0 are constants and T is temperature. This is shown in Figure 5a,b.

The results in Figure 5 show four important features.

First, all the measured FET mobility values for PFB and PFMO lie 100–1000 times below $\mu_{\text{FET}}(\text{model})$. Second, the measured FET mobility values do not obey the predicted power-law relationship from the model. Indeed, they do not obey any power-law, the FET mobility being approximately constant with increasing density on the log–log scale in Figure 5a,b. The same result was found for all PFB and PFMO transistors measured, both with and without OTS or FTP. Third, the values

of μ_{FET} (recorded at low fields) correspond well with $\mu_0(t_{1/4})$. PFMO is in excellent agreement, while PFB at $F = 2 \text{ kVcm}^{-1}$ is within a factor of 2. This is consistent with the results already discussed in Figure 4. Fourth, the DI and TOF mobility values at a given field for PFB do not vary with charge-carrier density; the smaller dataset for PFMO is consistent with this. This reflects the early discussion of the dark injection literature results.

Overall, the results in Figures 4 and 5 are consistent with a weakly field dependent, charge-carrier density independent mobility, in which transport at the dielectric interface in optimised transistors is the same as that in the bulk.

We do note that in the model of Tanase et al., the effect of dipolar disorder DOS broadening at the semiconductor-dielectric interface proposed by Veres et al.^[59] is not included. In this model static dipolar disorder in the dielectric increases the DOS width of the semiconductor in the FET channel. This would mean that $\sigma_{\text{DOS}}(\text{FET}) > \sigma_{\text{DOS}}$, increasing T_0 and the slope of $\mu_{\text{FET}}(\text{model})$. Considering Figure 5a,b, the inclusion of dipolar disorder DOS broadening would therefore make the model deviate even more from the experimentally measured μ_{FET} values.

Another key prediction of the charge-carrier density dependent mobility models is that the activation temperature for charge transport should decrease with increasing carrier density.^[9] One would expect the three orders of magnitude difference in carrier density to make the activation energy in the high-density transistor regime ($\approx 10^{19} \text{ cm}^{-3}$) approximately half that in the low-density diode regime ($\approx 10^{16} \text{ cm}^{-3}$).^[9] Temperature measurements were therefore conducted on PFB diodes and transistors in the range from 298 to 403 K (see Figure S6, Supporting Information). The zero-field TOF mobility was found to have an activation energy of 0.20 eV (GDM σ_{DOS} equivalent of 0.08 eV), the zero-field steady-state SCLC mobility giving similar values. The linear and saturation FET mobility were found to have an activation energy of 0.21 and 0.22 eV, respectively (GDM σ_{DOS} equivalents of 0.089 and 0.087 eV, respectively). This is not consistent with a charge-carrier density mobility. It is instead more consistent with a charge-carrier density independent mobility in which the energy landscape seen by the carriers does not change with density. Intriguingly, similar measurements of the well known vacuum sublimed glassy diamine small molecule *N,N'*-diphenyl-*N,N'*-bis(3-methylphenyl)-1-1'-biphenyl-4,4'-diamine show exactly the same result.^[60]

We also applied Equation (5) to the standard gradual channel approximation used to calculate transistor characteristics. For a constant mobility μ_{FET} this results in Equations (2a) and (2b). For a charge-carrier density dependent mobility given by Equation (5) this results instead in the approximate forms

$$I_D(\text{lin}) \approx \frac{W\mu_0 C_i}{L} \left(\frac{C_i}{e\Delta x p_0} \right)^m (V_G - V_T)^{m+1} V_D \quad (6a)$$

$$I_D(\text{sat}) = \frac{W\mu_0 C_i}{(m+2)L} \left(\frac{C_i}{e\Delta x p_0} \right)^m (V_G - V_T)^{m+2} \quad (6b)$$

(see Supporting Information, derivation S7). On a standard $I_D(\text{lin})$ versus V_G and $(I_D(\text{sat}))^{1/2}$ versus V_G plot, Equations (6a)

and (6b) should lead to nonlinear characteristics where both $I_D(\text{lin})$ and $(I_D(\text{sat}))^{1/2}$ follow a power-law with V_G . This can be taken as a marker of a charge-carrier density dependent mobility in any FET results. For a charge-carrier density independent mobility, $m = 0$ and Equations (6a) and (6b) reduce to Equations (2a) and (2b).

(However, we do note that the mobility-edge model, based on the relationship between free carriers in transport states and trapped carriers in an exponential distribution of deep states of characteristic temperature T_0 , produces exactly the same power-law relationships between $I_D(\text{lin})$ and V_G and $I_D(\text{sat})$ and V_G in Equations (6a) and (6b), with only the prefactors varying (see Supporting Information, derivation S8). This type of power-law relationship for discrete transport states with an exponential trap distribution has been noted previously and applied to pentacene OFETs by Horowitz et al.^[61])

P3HT was one of the polymers originally fitted to Equation (4) by Tanase et al.^[5] We measured the transfer characteristics of a reference sample of P3HT, and explored the applicability of Equations (6a) and (6b) (see Figure S9, Supporting Information). For this polycrystalline polymer, the $I_D(\text{lin})$ and $(I_D(\text{sat}))^{1/2}$ versus V_G characteristics are clearly nonlinear, and Equations (6a) and (6b) gave a good fit for $T_0 = 540$ K.

PFB and PFMO instead have highly linear $I_D(\text{lin})$ and $(I_D(\text{sat}))^{1/2}$ versus V_G characteristics (Figure 3c,d) and follow Equations (2a) and (2b). This is consistent with poly(triarylamine) and other fluorene-triarylamine copolymers, which also all have highly linear characteristics.^[38] Hence, the transfer characteristics alone indicate that the mobility of these polymers does not follow Equation (5).

If PFB and PFMO have a charge-carrier density independent mobility, the question arises as to how this can occur for a disordered amorphous material with a Gaussian DOS width of order 0.1 eV. A charge-carrier density dependent mobility works on the physical principal that as the carrier density increases, the probability of a deep site in the DOS sites being occupied by a carrier increases. Other carriers in the DOS are therefore less likely to visit those sites, and be slowed down by having to escape from them. The average mobility of the whole carrier ensemble therefore increases as their number increases. For a charge-carrier density independent mobility this cannot occur. The range of energies of the DOS sites visited by the carriers cannot vary as the number of carriers increases. The effective energy landscape needs to be much smoother.

One possibility is to include the effect of polarons. If the polaron activation energy is significant compared to the DOS width it would smooth out the energy landscape. It would also offer an elegant solution in explaining how density dependent and independent mobility materials can occur via the reorganization energy. TOF results for PFB and similar fluorene-triarylamine copolymers have been successfully fitted to the polaronic correlated GDM in the low-density regime, giving a polaron activation energy greater than the DOS width.^[43] For this situation, the multicarrier effective-medium approximation (EMA) analytical theory does indeed predict a charge-carrier density independent mobility, exactly as we observe.^[6] However, it also predicts a field-independent mobility, which we do not observe.^[12] A percolation model for transport in an uncorrelated Gaussian DOS also predicts a charge-carrier density dependent

mobility even with a polaronic contribution, suggesting this cannot explain the results in this work.^[8]

Another possibility is correlated disorder. With correlated disorder the nearest-neighbor transport site energies are correlated with each other, smoothing out the energy landscape as shown in Figure 1a. In an amorphous polymer this could be envisaged to occur by similarities in the nearest-neighbor chain conformation resulting in similarities in the conjugation length. This could again vary between different materials depending on backbone stiffness and interchain and sidegroup packing. TOF results for PFB and similar fluorene-triarylamine copolymers have been successfully fitted to the correlated GDM in the low-density regime.^[43] Steady-state SCLC diode measurements of fluorene-triarylamine copolymers have also been successfully fitted to the correlated and uncorrelated EGDM.^[44] The EGDM with correlated disorder (ECDM) does predict a mobility which is field dependent and charge-carrier independent (we note that analysis of the experimentally measured transport parameters for PFB and PFMO within the ECDM framework (see Supporting Information, Section S10) does, assuming an interchain hopping distance of 1 nm and a hopping attempt frequency of 10^{14} s⁻¹, yield not unreasonable values for the wavefunction decay length of 0.14–0.29 nm, respectively). The EMA theory with correlated disorder also predicts a mobility which is field dependent and effectively charge-carrier independent at the DOS widths found for PFB and PFMO.^[11] Hence, the presence of correlated disorder might offer a possible explanation of charge-carrier density independent transport in amorphous fluorene-triarylamine copolymers. Recent structural investigations of a noncrystalline high mobility polymer show long-range alignment between the chains.^[62] Such structural correlations may therefore be key to explaining charge transport in amorphous conjugated polymers.

3. Summary

We have investigated the charge-carrier density dependency of hole transport in two amorphous fluorene-triarylamine copolymer glasses. This is in both the low-density diode regime (10^{14} – 10^{17} cm⁻³) using TOF measurements and analysis of transient DI literature results, and in the high-density transistor regime (10^{17} – 10^{20} cm⁻³) using OFET measurements. We have also explored these results within the Vissenberg and Matters framework using the model developed by Tanase et al.^[5] This relates the magnitude and Gaussian DOS width for transport in the diode regime to the magnitude and exponential DOS density–mobility power-law for transport in the transistor regime.

First, we observe that: (i) the TOF transients of PFB and PFMO are nondispersive; (ii) the DI mobility for PFB does not vary with carrier density (the smaller dataset for PFMO is consistent with this). Both results are consistent with a density independent mobility in the low-density diode regime. Second, we observe that for PFB and PFMO the FET mobility remains approximately constant with carrier density. This is consistent with a density independent mobility in the high-density transistor regime. Third, we observe that: (i) for PFB and PFMO, the FET mobility for the best transistors is equal to the TOF

mobility at the same field; (ii) for PFB, the FET and TOF mobility have the same temperature dependency. Both results are consistent with a density independent mobility across both regimes. Fourth, we observe that for PFB and PFMO: (i) the FET mobility does not follow the density–mobility power-law predicted by the model; (ii) the magnitude of the FET mobility is two to three orders of magnitude below that predicted by the model. Both results are again consistent with a density independent mobility across both regimes.

Our results for these two amorphous fluorene-triarylamine copolymers are therefore consistent with a weakly field dependent, charge-carrier density independent mobility. This is unlike results for many other conjugated polymers, which appear to have a field dependent, charge-carrier density dependent mobility. We note that this density dependent mobility may also be a property linked to the polycrystalline morphology of many of these materials.

This charge-carrier density independent mobility could potentially be explained by correlated disorder in the fluorene-triarylamine copolymers. If molecular packing and backbone rigidity favor a more slowly varying chain morphology, nearest-neighbor conjugation lengths will be correlated, resulting in a smoothly varying transport state energy landscape. This suggests that long-range order is an important factor in determining charge transport in amorphous conjugated polymers.

4. Experimental Section

Time-of-Flight Measurements: Samples were prepared by spin-coating PFB and PFMO at 1500 rpm from *p*-xylene solutions at concentrations of 60–120 mg mL⁻¹. This was followed by a solvent removal baking step (100 °C, 10 min). TOF samples consisted of indium tin oxide (ITO) on glass substrates (purchased from CRL Optics; cleaned as described below for Si wafer substrates), spin-coated polymer films (thickness *d* of 1–2 μm as measured by a Dektak surface profiler), and thermally evaporated semitransparent (40 nm thick) Al top metal contacts. TOF measurements at room temperature and with temperature were conducted as described previously using a Quantel ND:YAG ns-pulsed laser (excitation wavelength 355 nm), an in-house fabricated DC source and a Tektronics TDS 3052 oscilloscope, and a helium exchange-gas Oxford Instruments Opstital cryostat.^[39,43]

Transistor Measurements: Samples were prepared by spin-coating PFB and PFMO at 3000 rpm from *p*-xylene, *o*-xylene, or chloroform solutions at concentrations of 5 or 10 mg mL⁻¹. This was followed by a solvent removal baking step (100 °C, 10 min). Film thicknesses were 40–60 nm (as measured by a Dektak surface profiler). FET samples consisted of standard Si (n⁺ doped)/SiO₂ wafer substrates with Au source and drain contacts (purchased from the Fraunhofer IPMS, Germany). Channel lengths *L* were 2.5, 5, 10, or 20 μm, channel widths *W* were 0.2, 1, or 2 cm, and SiO₂ thickness was 210 or 230 nm. The surface was cleaned prior to polymer deposition using a series of solvent washing and drying steps (water, acetone, and isopropyl alcohol (IPA); dried with pressurized N₂) followed by ozone plasma treatment for 10 min. For some devices, an OTS SAM was deposited on the SiO₂ surface (substrates immersed for 15 min at 60 °C in 10 × 10⁻³ M solution in toluene or hexadecane; then sequentially rinsed in toluene, acetone and IPA to remove excess material). For other devices, an FTP SAM was deposited on the surface of the Au contacts (substrates immersed for 14 h in 1 × 10⁻³ M solution in ethanol; then rinsed thoroughly in ethanol and cleaned in an ultrasonic bath to remove excess material). Contact angle measurements were used to confirm the presence and quality of the SAM layers using a Kruss drop shape analysis system. FET characteristics at room temperature and with temperature were recorded as described previously in a nitrogen

atmosphere (PFB and PFMO OTS, No SAM, FTP devices) or in ambient (PFB OTS devices were found to be ambient stable) using an Agilent 4155C or 4156C semiconductor parameter analyser, and a hot-stage mounted in a nitrogen filled glove box.^[57,63]

Materials: PFB and PFMO samples were supplied by the Sumitomo Chemical Co. The P3HT sample was supplied by Merck. All solvents and SAMs were purchased from Aldrich.

Materials Characterization: DSC measurements were carried out using a Mettler Toledo DSC1H at heating and cooling rates of 10 °C min⁻¹ using 2.12 and 2.23 mg of PFB and PFMO, respectively. Optical absorbance spectra were recorded using a Bentham single-beam UV–vis system. For the solution spectra, solutions were prepared at a concentration of 0.1 mg mL⁻¹ in toluene. For thin film spectra, films were made by drop-casting from 1 mg mL⁻¹ in toluene onto clean glass slides. XRD measurements used a Panalytical X'Pert Pro diffractometer operating at 40 kV and 40 mA with Ni filtered CuKα radiation. The PFB was cast from 38 mg mL⁻¹ in toluene solution via spin-coating and then annealed for 1 h at 150 °C (above the glass transition at 132 °C). Film thickness was measured to be 330 nm.

Supporting Information

Supporting Information is available from the Wiley Online Library or from the author.

Open data statement: the underlying data supporting this publication is available upon request at datainquiryEXSS@imperial.ac.uk.

Acknowledgements

The authors would like to thank the Sumitomo Chemical Co for supplying PFB and PFMO samples and Merck for supplying the P3HT sample. They also thank the UK Engineering and Physical Sciences Research Council (UK EPSRC) for funding Ruth Rawcliffe (Award Number GR/P00772/01), Alexander Guite (Award Number EP/P502500/1), and Abhimanyu Mukherjee (Award Number EP/M506345/1) through Doctoral Training Award studentships and Jorge C. D. Faria (Award Number EP/G037515/1) through a Plastic Electronics Doctoral Training Centre studentship. Donal Bradley thanks the Lee-Lucas endowment for support.

Received: November 3, 2015

Revised: January 15, 2016

Published online:

- [1] H. Bässler, *Phys. Stat. Sol. (B)* **1993**, 175, 15.
- [2] S. V. Novikov, D. H. Dunlap, V. M. Kenkre, P. E. Parris, A. V. Vannikov, *Phys. Rev. Lett.* **1998**, 81, 4472.
- [3] P. E. Parris, V. M. Kenkre, D. H. Dunlap, *Phys. Rev. Lett.* **2001**, 87, 126601.
- [4] M. C. J. M. Vissenberg, M. Matters, *Phys. Rev. B* **1998**, 57, 12964.
- [5] C. Tanase, E. J. Meijer, P. W. M. Blom, D. M. de Leeuw, *Phys. Rev. Lett.* **2003**, 91, 216601.
- [6] I. I. Fishchuk, V. I. Arkhipov, A. Kadashchuk, P. Heremans, H. Bässler, *Phys. Rev. B* **2007**, 76, 045210.
- [7] W. F. Pasveer, J. Cottaar, C. Tanase, R. Coehoorn, P. A. Bobbert, P. W. M. Blom, D. M. de Leeuw, M. A. J. Michels, *Phys. Rev. Lett.* **2005**, 94, 206601.
- [8] J. Cottaar, L. J. A. Koster, R. Coehoorn, P. A. Bobbert, *Phys. Rev. Lett.* **2011**, 107, 136601.
- [9] I. I. Fishchuk, A. Kadashchuk, J. Genoe, M. Ullah, H. Sitter, Th. B. Singh, N. S. Sariciftci, H. Bässler, *Phys. Rev. B* **2010**, 81, 045202.

- [10] M. Bouhassoune, S. L. M. van Mensfoort, P. A. Bobbert, R. Coehoorn, *Org. Elec.* **2009**, *10*, 437.
- [11] I. I. Fishchuk, A. Kadashchuk, M. Ullah, H. Sitter, A. Pivrikas, J. Genoe, H. Bäessler, *Phys. Rev. B* **2012**, *86*, 045207.
- [12] I. I. Fishchuk, A. Kadashchuk, V. N. Poroshin, H. Bäessler, *Phil. Mag.* **2010**, *90*, 1229.
- [13] C. Tanase, P. W. M. Blom, D. M. de Leeuw, E. J. Meijer, *Phys. Stat. Sol. (A)* **2004**, *201*, 1237.
- [14] I. Katsouras, A. Najafi, K. Asadi, A. J. Kronemeijer, A. J. Oostra, L. J. A. Koster, D. M. de Leeuw, P. W. M. Blom, *Org. Elec.* **2013**, *14*, 1591.
- [15] T. Leijtens, J. Lim, J. Teuscher, T. Park, H. J. Snaith, *Adv. Mater.* **2013**, *25*, 3227.
- [16] H. Sirringhaus, P. J. Brown, R. H. Friend, M. M. Nielsen, K. Bechgaard, B. M. W. Langeveld-Voss, A. J. H. Spiering, R. A. J. Janssen, E. W. Meijer, P. Herwig, D. M. de Leeuw, *Nature* **1999**, *401*, 685.
- [17] A. R. Aiyar, J.-I. Hong, R. Nambiar, D. M. Collard, E. Reichmanis, *Adv. Funct. Mater.* **2011**, *21*, 2652.
- [18] E. J. W. Crossland, K. Tremel, F. Fischer, K. Rahimi, G. Reiter, U. Steiner, S. Ludwigs, *Adv. Mater.* **2012**, *24*, 839.
- [19] H. Yang, E. Glynos, B. Huang, P. F. Green, *J. Phys. Chem.* **2013**, *117*, 9590.
- [20] C. Y. Yang, F. Hide, M. A. Diaz-Garcia, A. J. Heeger, Y. Cao, *Polymer* **1998**, *39*, 2299.
- [21] A. R. Inigo, C. C. Chang, W. Fann, J. D. White, Y. S. Huang, U. S. Jeng, H. S. Sheu, K. Y. Peng, S. A. Chen, *Adv. Mater.* **2005**, *17*, 1835.
- [22] Y. F. Huang, A. R. Inigo, C. C. Chang, K. C. Li, C. F. Liang, C. W. Chang, T. S. Lim, S. H. Chen, J. D. White, U. S. Jeng, A. C. Su, Y. S. Huang, K. Y. Peng, S. A. Chen, W. W. Pai, C. H. Lin, A. R. Tameev, S. V. Novikov, A. V. Vannikov, W. S. Fann, *Adv. Funct. Mater.* **2007**, *17*, 2902.
- [23] U. Jeng, C.-H. Hsu, H.-S. Sheu, H.-Y. Lee, A. R. Inigo, H. C. Chiu, W. S. Fann, S. H. Chen, A. C. Su, T.-L. Lin, K. Y. Peng, S. A. Chen, *Macromolecules* **2005**, *38*, 6566.
- [24] M. Morana, M. Wegscheider, A. Bonanni, N. Kopidakis, S. Shaheen, M. Scharber, Z. Zhu, D. Waller, R. Gaudiana, C. Brabec, *Adv. Funct. Mater.* **2008**, *18*, 1757.
- [25] C. Elschner, A. A. Levin, L. Wilde, J. Grenzer, C. Schroer, K. Leoa, M. Riede, *J. Appl. Cryst.* **2011**, *44*, 983.
- [26] R. Matsubara, M. Sakai, K. Kudo, N. Yoshimoto, I. Hirose, M. Nakamura, *Org. Electron.* **2011**, *12*, 195.
- [27] R. Noriega, J. Rivnay, K. Vandewal, F. P. V. Koch, N. Stingelin, P. Smith, M. F. Toney, A. Salleo, *Nat. Mater.* **2013**, *12*, 1038.
- [28] S. Yogev, R. Matsubara, M. Nakamura, Y. Rosenwaks, *Org. Electron.* **2010**, *11*, 1729.
- [29] A. Salleo, T. W. Chen, A. R. Völkel, Y. Wu, P. Liu, B. S. Ong, R. A. Street, *Phys. Rev. B* **2004**, *70*, 115311.
- [30] R. A. Street, J. E. Northrup, A. Salleo, *Phys. Rev. B* **2005**, *71*, 165202.
- [31] M. Redecker, D. D. C. Bradley, M. Inbasekaran, W. W. Wu, E. P. Woo, *Adv. Mater.* **1999**, *11*, 241.
- [32] M. J. Harding, D. Poplavskyy, V. E. Choong, A. J. Campbell, *Adv. Funct. Mater.* **2010**, *20*, 119.
- [33] J. C. D. Faria, A. J. Campbell, M. A. McLachlan, *J. Mater. Chem. C* **2015**, *3*, 4945.
- [34] J. C. D. Faria, A. J. Campbell, M. A. McLachlan, *Adv. Funct. Mater.* **2015**, *25*, 4657.
- [35] A. C. Morteani, A. S. Dhoot, J.-S. Kim, C. Silva, N. C. Greenham, C. Murphy, E. Moons, S. Cina, J. H. Burroughes, R. H. Friend, *Adv. Mater.* **2003**, *15*, 1708.
- [36] J.-S. Kim, L. Lu, P. Sreearunothai, A. Seeley, K.-H. Yim, A. Petrozza, C. E. Murphy, D. Beljonne, J. Cornil, R. H. Friend, *J. Am. Chem. Soc.* **2008**, *130*, 13120.
- [37] J.-S. Kim, R. H. Friend, I. Grizzi, J. H. Burroughes, *Appl. Phys. Lett.* **2005**, *87*, 023506.
- [38] W. Zhang, J. Smith, R. Hamilton, M. Heaney, J. Kirkpatrick, K. Song, S. E. Watkins, T. Anthopoulos, I. McCulloch, *J. Am. Chem. Soc.* **2009**, *131*, 10814.
- [39] D. Poplavskyy, J. Nelson, D. D. C. Bradley, *Macromol. Symp.* **2004**, *212*, 415.
- [40] A. Papadimitratos, H. H. Fong, G. G. Malliaris, A. Yakimov, A. Duggal, *Appl. Phys. Lett.* **2007**, *91*, 042116.
- [41] A. J. Campbell, D. D. C. Bradley, H. Antoniadis, M. Inbasekaran, W. W. Wu, E. P. Woo, *Appl. Phys. Lett.* **2000**, *76*, 1734.
- [42] S. Logan, J. E. Donaghey, W. Zhang, I. McCulloch, A. J. Campbell, *J. Mater. Chem. C* **2015**, *3*, 7526.
- [43] R. U. A. Khan, D. Poplavskyy, T. Kreouzis, D. D. C. Bradley, *Phys. Rev. B* **2007**, *75*, 035215.
- [44] R. J. de Vries, S. L. M. van Mensfoort, V. Shabro, S. I. E. Vulto, R. A. J. Janssen, R. Coehoorn, *Appl. Phys. Lett.* **2009**, *94*, 163307.
- [45] M. Bernius, M. Inbasekaran, E. Woo, W. Wu, L. Wujkowski, *J. Mater. Sci.: Mater. Electron.* **2000**, *11*, 111.
- [46] Y. Zhao, G. Yuan, P. Roche, M. Leclerc, *Polymer* **1995**, *36*, 2211.
- [47] S. H. Chen, A. C. Su, C. H. Su, S. A. Chen, *Macromolecules* **2005**, *38*, 379.
- [48] C. L. Donley, J. Zaumseil, J. W. Andreasen, M. M. Nielsen, H. Sirringhaus, R. H. Friend, J.-S. Kim, *J. Am. Chem. Soc.* **2005**, *127*, 12890.
- [49] G. C. Faria, E. R. de Azevedo, H. von Seggern, *Macromolecules* **2013**, *46*, 7865.
- [50] O. Werzer, H.-G. Flesch, D.-M. Smilgies, R. Resel, *J. Polym. Sci.: Part B: Polym. Phys.* **2009**, *47*, 1599.
- [51] L. Kindera, J. Kanickia, P. Petroff, *Synth. Met.* **2004**, *146*, 181.
- [52] F. C. Spano, *Chem. Phys.* **2006**, *325*, 22.
- [53] J. Clark, J.-F. Chang, F. C. Spano, R. H. Friend, C. Silva, *Appl. Phys. Lett.* **2009**, *94*, 163306.
- [54] M. Grell, D. D. C. Bradley, X. Long, T. Chamberlain, M. Inbasekaran, E. P. Woo, M. Soliman, *Acta Polym.* **1998**, *49*, 439.
- [55] D. Liu, R. O. Orozco, T. Wang, *Phys. Rev. E* **2013**, *88*, 022601.
- [56] P. W. M. Blom, C. Tanase, D. M. de Leeuw, R. Coehoorn, *Appl. Phys. Lett.* **2005**, *86*, 092105.
- [57] R. Rawcliffe, M. Shkunov, M. Heaney, S. Tierney, I. McCulloch, A. J. Campbell, *Chem. Commun.* **2008**, *7*, 871.
- [58] Robert Peter Stanley, *PhD Thesis*, Imperial College London **2012**.
- [59] J. Veres, S. D. Ogier, S. W. Leeming, D. C. Cupertino, S. M. Khaffaf, *Adv. Funct. Mater.* **2003**, *13*, 199.
- [60] C. H. Cheung, K. K. Tsung, K. C. Kwok, S. K. So, *Appl. Phys. Lett.* **2008**, *93*, 083307.
- [61] G. Horowitz, P. Lang, M. Mottaghi, H. Aubin, *Adv. Funct. Mater.* **2004**, *14*, 1069.
- [62] X. Zhang, H. Bronstein, A. J. Kronemeijer, J. Smith, Y. Kim, R. J. Kline, L. J. Richter, T. D. Anthopolous, H. Sirringhaus, K. Song, M. Heaney, W. Zhang, I. McCulloch, D. M. DeLongchamps, *Nat. Commun.* **2013**, *4*, 2238.
- [63] X. Wang, K. Wasapinyokul, W. D. Tan, R. Rawcliffe, A. J. Campbell, D. D. C. Bradley, *J. Appl. Phys.* **2010**, *107*, 024509.